Highly efficient and stable solid-state luminescent nanohybrids: Precise architecture and enhancement mechanism

Ya Kun Zhu
State Key Laboratory for Modification of Chemical Fibers and Polymer Materials & College of Material Science and Engineering, Donghua University, Shanghai 201620, China

Shan Yi Guang
College of Chemistry and Chemical Engineering & Bioengineering, Donghua University, Shanghai 201620, China

Xin Yan Su and Hong Yao Xu[a)]
State Key Laboratory for Modification of Chemical Fibers and Polymer Materials & College of Material Science and Engineering, Donghua University, Shanghai 201620, China; and College of Materials Science and Engineering, Shanghai University, Shanghai 201800, People's Republic of China

Xiang Yang Liu
The Department of Physics, National University of Singapore, Singapore 1175542

(Received 13 November 2012; accepted 18 January 2013)

The organic light-emitting (OLE) materials have attracted great interest due to their potential applications in sensors, biodetectors and OLE devices. However, highly efficient emission from organic solids is still a great challenge because of the aggregation-caused quenching effect. In this article, a three-dimensional (3D) organic-inorganic hybrid nanoparticle, based on polyhedral oligomeric silsesquioxane (POSS), was precisely fabricated via click chemistry with high yield, and its structure was characterized by Fourier transform infrared spectroscopy, ^{1}H, and ^{29}Si nuclear magnetic resonance spectroscopies, and Matrix-Assisted Laser Desorption Ionization Time-of-Flight Mass Spectrometry, respectively. The resultant 3D organic-inorganic nanohybrid showed significantly enhanced emission in solid film (Φ_{film} 80%) with a slight red-shift as compared with its organic counterpart, (Φ_{film} 14%), which exhibits a large red-shift in solid film, due to the deaggregation effect of POSS. Simultaneously, the resultant nanohybrid also exhibited good film formability, excellent spectrum and thermal stability (>250 °C) due to the introduction of POSS.

I. INTRODUCTION

Organic light-emitting (OLE) materials have received considerable interest due to their promising application in biodetectors, sensors and organic light-emitting devices (OLEDs).[1–3] However, the conjugated coplanar structures of OLE materials lead to aggregation-caused quenching (ACQ) effect in solid state due to strong intermolecular dipole-dipole and π-π stacking interaction, which severely limits their practical applications.[4–7] Three-dimensional (3D) structural molecules with a large space free volume, such as hyperbranch and dendrimer, provide an important means to reduce and eliminate the aggregation due to steric hindrance effect.[8–13] However, these resultant 3D materials often show low thermal properties. Simultaneously, the difficulty experienced during synthesis and purification also limits their practical applications.

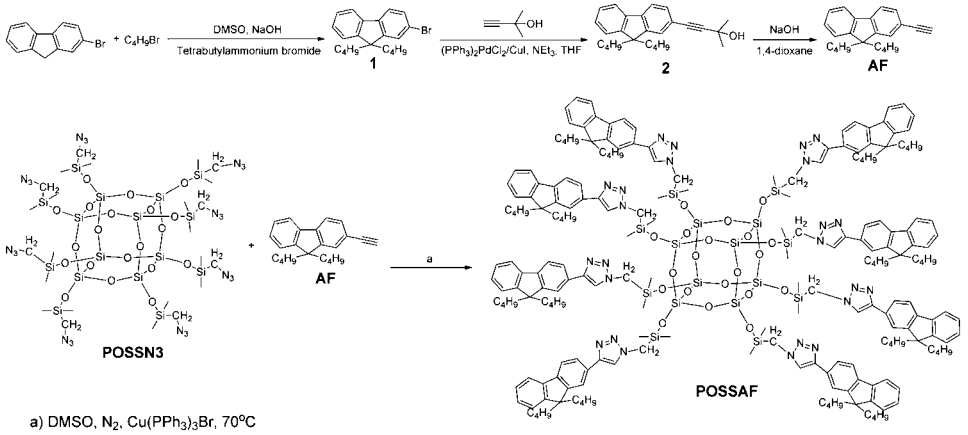
Fortunately, the discovery of click chemistry method and polyhedral oligomeric silsesquoixanes (POSS) with special 3D cage-like nanoscale structure provides an important means to solve these problems. Click chemistry, especially 1,3-dipolar cycloaddition reaction between azide and alkynes to form a stable 1,2,3-triazole linked compound, has received considerable attention because of some outstanding advantages such as mild reaction conditions, excellent tolerance of oxygen and water, high yields, simple isolation procedure, and almost perfect stereoselectivity.[14] And POSS is a nanometer-sized cube-like molecule with inorganic core surrounded by eight organic corner groups (active or inert), which have been demonstrated to be excellent platforms and building blocks for the architecture of novel 3D organic-inorganic molecular hybrid materials.[15–17] Many POSS-based hybrids have been prepared and are found to possess improved properties when compared with their organic counterparts.[18–22] In our recent work, some functional POSS-based hybrid materials with low dielectric constant or enhanced nonlinear optical properties were reported.[22–26]

In this work, a well-defined 3D nanoscale dendritic hybrid, octakis(4-(9,9-dibutylfluorene)-1-methyl)-1,2,3-triazole-(dimethylsiloxy)octa-silsequioxane (POSSAF) (Sch. 1) has been designed and precisely prepared via click chemistry. The improvement mechanism of photophysical

[a)]Address all correspondence to this author.
e-mail: hongyaoxu@163.com
DOI: 10.1557/jmr.2013.36

https://doi.org/10.1557/jmr.2013.36 Published online by Cambridge University Press

 © Materials Research Society 2013



SCHEME 1. The synthetic route of 3D nanoscale dendritic hybrid POSSAF.

properties, thermal and optical stability, and film formability after introduction of POSS was systematically investigated.

II. EXPERIMENTAL SECTION

A. Materials and measurements

Octakis(azidomethyl)(dimethylsiloxy)octasilsesquioxane ($POSSN_3$) and 2-ethynyl-9,9- dibutylfluorene (AF) were synthesized by our group.[27] $Cu(PPh_3)_3Br$ was prepared in accordance with the Ref. 28. $PdCl_2(PPh_3)_2$ and 2-methylbut-3-yn-2-ol were purchased from J & K Scientific Ltd. (Shanghai, China). 2-bromofluorene was obtained from TEIKO International Ltd. (Shanghai, China). 1-Bromooctane, sodium hydroxide (NaOH), tetrabutylammonium bromide, dimethyl sulfoxide (DMSO), tetrahydrofuran (THF), triethylamine (TEA), 1,4-dioxane and N,N-dimethylformamide (DMF) were purchased from Shanghai Chemical Reagent Company (Shanghai, China). All commercial reagents were used as received except that THF and TEA were distilled immediately prior to use.

Fourier transform infrared spectra were recorded as KBr disk on (FTIR; Nicolet model No. NEXUS 8700 FTIR, Waltham, MA) spectrometer. Temperature-dependent FTIR were tested at each temperature for 30 min in air. ^1H nuclear magnetic resonance spectra were collected on (NMR; Bruker model No. DMX-400, Frankfurt, Germany) spectrometer using chloroform-*d* ($CDCl_3$) as a solvent. Solid-state ^{29}Si nuclear magnetic resonance measurements were carried out at room temperature using (NMR; Bruker model No. DMX-400, Frankfurt, Germany) spectrometer at a resonance frequency of 79.49 MHz. Matrix-assisted laser desorption ionization time-of-flight mass spectrometry was performed using the spectrometer (MALDI-TOF-MS; model No. Voyager-DE RP, Huntsville, AL) in linear and reflectron modes. The matrix 2,5-dihydroxybenzoic acid (DHBA) was dissolved in THF (10 mg/mL), and mixed with the sample solution (0.5–1 mg/mL in THF) in 1:1 v/v ratio. The samples were deposited on the target and dried in air. The matrix 2,5-dihydroxybenzoic acid (DHBA) was dissolved in THF (10 mg/mL), and mixed with the sample solution (0.5–1 mg/mL in THF) in 1:1 v/v ratio. The samples were deposited on the target and dried in air. Elemental analyses were performed by CHNOS Elemental Analyzer, Vario El III (Elementar, Germany). The optical properties of the sample were measured by TU-1901 ultraviolet-visible (UV-Vis) spectrophotometer and PF-6600 Fluorescence spectrometer (JASCO, Japan) with a 1-cm quartz cell in tetrahydrofuran (THF, 1×10^{-6} M). The concentration (C%) of POSSAF in THF was calculated using organic chromophore arm numbers as standard, namely $C_{sol} = C_{POSSAF} \times 8$. For the thin film spectra, hybrid was first dissolved in chloroform (1 wt%) and then spin-coated on quartz plates at 1000 rpm for 30 s. Then, the film samples were dried at 50 °C under vacuum. Quantum efficiency (QE, Φ) was determined by a modification of the relative method described by Demas and Crosby using 9, 10-diphenylanthracence (90%) as in Ref. 29. QE of materials in film was recorded by using 9,10-diphenylanthrancene [dispersed in polymethylmethacrylate (PMMA) films with a concentration lower than 1×10^{-3} M and a photoluminescence quantum efficiency (PLQE) of 83%] as a standard. The atomic force microscopic images of films were made in the trapping mode (AFM; Agilent model No. 5500 AFM, Santa Clara, CA). Optical microscopic images of films were taken in a (OM; model No. CMM-88E, Beijing, China) metallographic microscope. For investigating the thermal stability of the prepared hybrid materials, films were annealed on a hot plate in air at 100 °C for 1 h, each. Thermogravimetric analysis was performed on a (TGA; TA Instruments model No. TGA 2050, New Castle, DE) TGA under a N_2 atmosphere at a heating rate of 10 °C/min. The calorimetry was carried on a differential scanning calorimeter (DSC; TA Instruments model No. DSC 9000, New Castle, DE) equipped with a liquid nitrogen cooling accessory (LNCA) unit under a continuous nitrogen purge (40 mL/min).

https://doi.org/10.1557/jmr.2013.36 Published online by Cambridge University Press

B. Synthesis

1. 2-bromo-9,9-dibutylfluorene (1)

2-dibromofluorene (4.9 g, 20 mmol) and tetrabutyl ammonium bromide (38 mg, 0.16 mmol) were dissolved in 100 mL DMSO. After the reaction mixture was stirred vigorously for 10 min, 7 mL of 0.5 M aqueous NaOH solution and 1-bromobutane (4.8 mL, 45 mmol) were added drop wise to the mixture. The reaction mixture was stirred at room temperature for 3 h. A precipitate was formed by adding 500 mL water and filtered off. The solid was recrystallized from n-hexane to give white crystals (95%). mp 66 °C; ^{1}H NMR (400 MHz, $CDCl_3$, δ): 7.64–7.66 (m, 1H, Ar–H), 7.53–7.55 (d, 1H, Ar–H), 7.42–7.45 (m, 2H, Ar–H), 7.30–7.31 (m, 3H, Ar–H), 1.90–1.95 (m, 4H, CH_2), 1.04–1.26 (m, 4H, CH_2), 0.82 (t, 6H, J = 7.1 Hz, CH_3), 0.57–0.60 (m, 4H, CH_2); FTIR (cm^{-1}, KBr): 2927, 2854 (s; CH_2), 1462, 1112 (m; Ar). Anal. Calcd. For $C_{21}H_{25}Br$: C, 70.59; H, 7.05. Found: C, 72.17; H, 7.06.

2. 4-(9,9-dibutyl-9H-fluoren-2-yl)-2-methylbut-3-yn-2-ol (2)

Under nitrogen, a mixture of compounds 2-bromo-9,9-dibutylfluorene (0.18 g, 0.5 mmol), 2-methylbut-3-yn-2-ol (0.4 mL, 4 mmol), $PdCl_2(PPh_3)_2$ (14 mg, 0.02 mmol) and CuI (2 mg, 0.01 mmol) were dissolved in 10 mL TEA and 10 mL THF. The reaction mixture was refluxed at 70 °C for 10 h. After cooling to room temperature, the insolubles were filtered off. After the removal of the solvent with a rotary evaporator, water and CH_2Cl_2 were added to the mixture, and the organic phase was purified by column chromatrography on silica gel with ethyl acetate/petroleum ether mixture (1:10 v/v) to give with yellow crystals (85%). mp 57 °C; ^{1}H NMR (400 MHz, $CDCl_3$, δ): 7.61–7.68 (m, 2H, Ar–H), 7.39–7.41 (m, 2H, Ar–H), 7.31–7.33 (m, 3H, Ar–H), 2.08 (s, 1H, OH), 1.94 (t, 4H, J = 7.7 Hz, CH), 1.66 (s, 6H, CH_3), 1.02–1.25 (m, 4H, CH_2), 0.82 (t, 6H, J = 7.1 Hz, CH_3), 0.55–0.58 (m, 4H, CH_2); FTIR (cm^{-1}, KBr): 3378 (m; –OH), 2927, 2852 (s; –CH_2), 2228 (w; C≡C), 1458, 1166 (m; Ar–H). Anal. Calcd. For $C_{26}H_{32}O$: C, 86.62; H, 8.95. Found: C, 88.13; H, 8.89.

3. 2-ethynyl-9,9-dibutylfluorene (AF)

Under nitrogen, a mixture of compound 2-(2-methyl-3-butyne-2-ol)-9,9-dibutylfluorene (0.1 g, 0.25 mmol), NaOH (4.8 g, 1.2 mmol) was added into 20 mL 1,4-dioxane. The reaction mixture was refluxed at 80 °C for 4 h. After cooling to room temperature, water and CH_2Cl_2 were added to the mixture, and the organic phase purified by column chromatography on silica gel with ethyl acetate/petroleum ether mixture (1:6 v/v) to give with yellow crystals (95%). mp 70 °C; ^{1}H NMR (400 MHz, $CDCl_3$, δ): 7.66–7.74 (m, 2H, Ar–H), 7.51–7.53 (m, 2H, Ar–H), 7.32–7.39 (m, 3H, Ar–H), 3.16 (s, 1H, C≡CH), 1.97–2.02 (m, 4H, CH_2), 1.08–1.32 (m, 4H, CH_2), 0.86 (t, 6H, J = 7.1 Hz, CH_3), 0.59–0.69 (m, 4H, CH_2); FTIR (cm^{-1}, KBr): 3275 (s; C≡C–H), 2954, 2924, 2854 (s; –CH_2), 2099 (w; C≡C), 1451, 1126 (m; Ar–H). Anal. Calcd. For $C_{23}H_{26}$: C, 91.34; H, 8.66. Found: C, 91.13; H, 8.87.

4. Click synthesis of POSSAF

0.14 g of octakis[dimethyl(p-azidomethylene)siloxyl] octasilsesquioxane ($POSSN_3$) (0.1 mmol), 0.24 g of 9,9-dibutylfluorene (AF) (0.8 mmol) and 0.01 g of Cu$(PPh_3)_3$Br (0.08 mmol) catalyst in 10 mL DMF were stirred for 10 h at 70 °C under N_2. Then the resultant mixture was dropped into EDTA saturated aqueous solution to precipitate the product. A white powder was collected by filtration. The crude product was purified by flash silica gel column chromatography using CH_2Cl_2 as the eluting solvent to obtain a white solid in ~90% yield. ^{1}H NMR (400 MHz, $CDCl_3$, δ): 0.30 (48H, s, H^a), 0.52–0.70 (m, 64H, $H^{m,n}$), 1.02–1.13 (m, 32H, H^l), 1.95–2.10 (m, 32H, H^k), 4.59 (s, 16H, Hb), 7.30–7.41 (32H, m, H^{g-j}), 7.65–7.78 (32H, m, H^{c-f}); ^{29}Si NMR (solid, δ): 9.1 (8Si, s, -OSi(Me)$_2$), -110.1 (8Si, s, –O–Si–O–); MALDI-TOF MS $[C_{208}H_{272}N_{24}O_{20}Si_{16}+Na]+$: Calcd. 3900.90, found 3900.09. Anal. Found: C, 64.72; H, 7.014; O, 8.02%. Calcd for $C_{208}H_{272}N_{24}O_{20}Si_{16}$: C, 64.42; H, 7.07; O, 8.25%.

III. RESULTS AND DISCUSSION

A. Click synthesis and structure characterization

The 3D POSS-based nanoparticle was precisely prepared using AF and $POSSN_3$ as raw materials through a Click reaction between N_3 and C≡C bond according to the literature.[30,31] To avoid the forming of cross-linked gel during treatment, which is insoluble and infusible, a organosoluble Cu$(PPh_3)_3$Br was selected as a catalyst instead of $CuSO_4$/sodium ascorbate.

The resultant POSSAF is soluble in some common organic solvents such as chloroform, THF, DMF, DMSO etc. POSSAF and the intermediates were characterized by FTIR, ^{1}H NMR, ^{29}Si NMR, elemental analyses, and MALDI-TOF MS, and satisfactory analytic data corresponding to their molecular structures were obtained, demonstrating that the resultant POSSAF was successfully prepared. All the characteristic data were given in Sec. II. B and Fig. 1. Figure 1(a) is the FTIR spectra of AF, $POSSN_3$ and POSSAF. As shown in Fig. 1(a), the characteristic absorptions of AF at 3275, 2099 cm^{-1} responding to ≡C–H, C≡C stretching vibration absorption and the stretching vibration at 2098 cm^{-1} of $POSSN_3$ assigned to the strong –N_3 absorption completely disappear in the FTIR spectrum of POSSAF while the characteristic Si–O–Si stretching vibration of POSS core still exists. Simultaneously, a new absorption band at 1623 cm^{-1} appears in the FTIR spectrum of POSSAF, which is assigned to the stretching

https://doi.org/10.1557/jmr.2013.36 Published online by Cambridge University Press

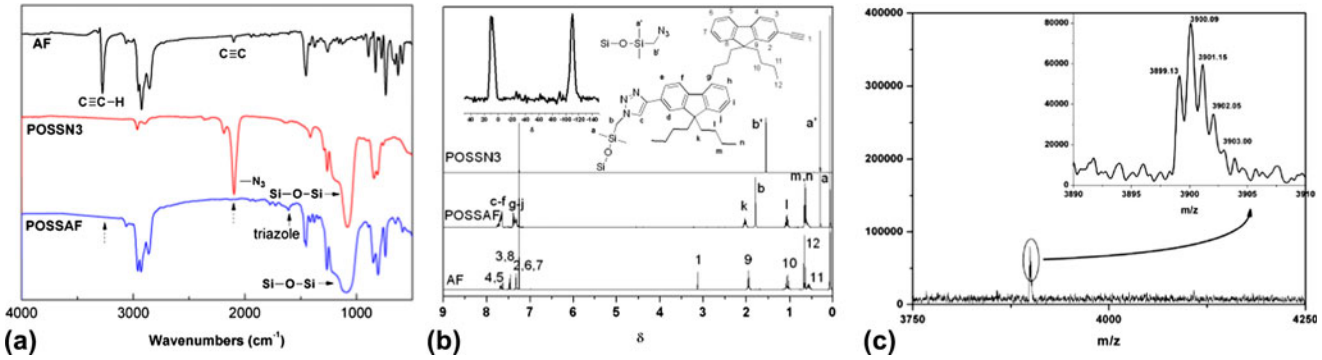


FIG. 1. The (a) FTIR (b) ^{1}H NMR and (the inset) ^{29}Si NMR spectra of AF, POOSN$_3$ and POSSAF. (c) MALDI-TOF MS of POSSAF.

vibration of triazole ring, indicating that all the eight azide groups of POSSN$_3$ completely reacted with alkynyl groups of AF to form POSSAF at almost stoichiometric pattern. In ^{1}H NMR spectra [Fig. 2(b)], it is also found that the characteristic alkyne proton absorption located at 3.13 ppm in the spectrum of AF completely disappears after click chemistry reaction and new vibration bands at 4.59 ppm (–SiCH$_2$) and 0.29 ppm (–SiCH$_3$) turn up in the ^{1}H NMR spectrum of POSSAF, further confirming that the targeted nanohybrid molecule has been obtained. In addition, the ^{29}Si NMR spectrum of POSSAF [Fig. 2(b), inset] exhibits two characteristic spectral peaks with almost equal area at 9.1 and −110.1 ppm, assigned to the Q- and T-type Si of the spherosilicate, respectively, indicating that there are two types of Si atoms at 1:1 ratio in the resultant hybrid, confirming that the resultant nanoparticles keep the POSS cages intact. Moreover, the results from C, H, N element analyses almost completely agree with the theoretically calculated values of targeted nanohybrid compound. Most importantly, in Fig. 1(c), the result of MALDI-TOF MS provides further evidence that the target molecule was formed [m/z = 3900.90, corresponding to $(M+Na)^{+}$].

B. Optical properties—UV-Vis and fluorescence spectroscopy

UV-Vis and fluorescence spectra of AF and POSSAF in THF with concentration of 1.0×10^{-6} mol/L are provided in Fig. 2. As is shown in the spectra, the maximum absorption peak of AF is at 288 nm. And after clicking with POSSN3, the maximum absorption peak of POSSAF only red-shifts to 290 nm, which is due to a nonoptimal conjugation of the 1H-1,2,3-triazole moiety.[32] And the tiny red-shift also indicates that the introduction of the silsesquioxane segment has no significant effect on the electron distribution of POSSAF. Similar results were found in the literature.[33] Similar red-shift phenomenon was also observed in their emission spectra. Meanwhile, POSSAF shows a pure UV emission (main emission spectrum <400 nm), which is hardly achieved from organic light-emitting materials due to the contradiction of molecular

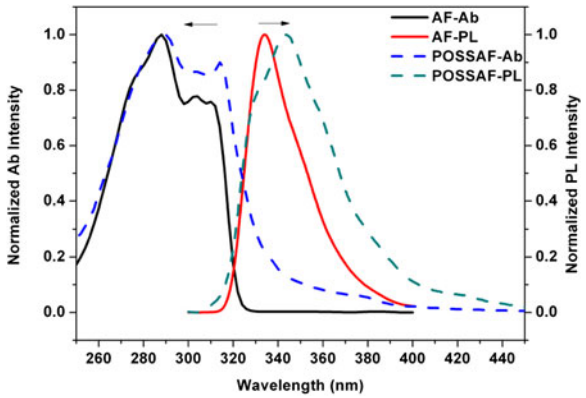


FIG. 2. The normalized absorption and emission spectra of AF and POSSAF.

design: to realize UV emission, there is a need to restrain the conjugation extent of organic molecule, whereas, the small conjugated molecular size often leads to the instability of materials both in structures and properties. The pure UV emission of POSSAF may be due to two reasons. On the one hand, POSS commonly has no impact on the photophysical properties of the organic component owing to its large highest occupied molecular orbital (HOMO)- lowest unoccupied molecular orbital (LUMO) gap, ~6.85 eV[34]; on the other hand, the –CH$_2$ group effectively breaks the conjugation between Si atom and organic unit. Furthermore, POSSAF shows a slight increase of fluorescence quantum yield in dilute solution compared with AF (84% and 83%, respectively). The slight difference may be due to the enhancement effect of POSS. However, this enhancement is not obvious in dilute solution, which is remarkable in solid film and is investigated in detail in the following text.

C. Computational analysis of nanoparticle and electron distribution

For validating the rationality of structural design of the organic nanoparticle, the theoretical calculation was

https://doi.org/10.1557/jmr.2013.36 Published online by Cambridge University Press

conducted using the Gaussian 03 software suite of the B3LYP/6-31G level of theory.[35] For simplifying the calculation, single-arm structural unit was selected and the bonds at the other seven end of the POSS cage were saturated with hydrogen atoms. The calculated results are shown in Fig. 3. It is found that the chromophoric molecular charge is mainly distributed on organic arms, that is, the HOMO and the LUMO of POSSAF are localized at each organic arm. These results further confirm that the introduction of POSS cages has no marked influence on electron distribution and can efficaciously ensure the light emission purity.

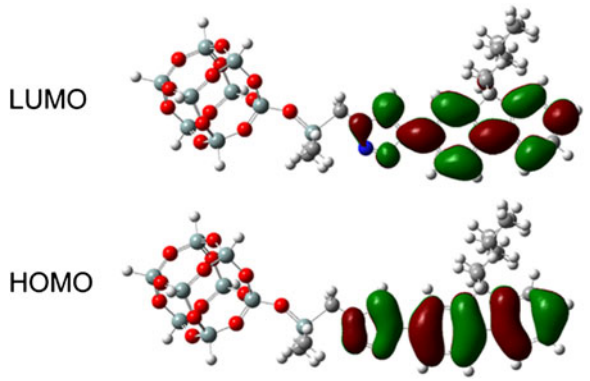


FIG. 3. Modeling of molecular orbital for POSSAF.

D. Film formability of POSSAF

The film formability of POSSAF is crucial for rationally investigating the light-emitting properties in solid state as well as further applications. Therefore, the microstructure and film formability of POSSAF was investigated.

Although both AF and POSSAF have good solubility in $CHCl_3$, only POSSAF can be spin-coated to excellent film. Thin films of AF and POSSAF were prepared by spin-coating method (solution concentration ~10 mg/mL) on quartz plates at 1000 rpm for 30 s. And to ensure the accuracy of measurement, three samples of both were prepared. As seen in Fig. 4, The AFM images and OM micrographs of POSSAF show that the surfaces of POSSAF films are quite smooth and no cracks and aggregation are observed. However, AF could not form satisfactory films and obvious cracks and aggregation were observed by metallurgical microscope. And even satisfactory AFM data of AF film cannot be obtained due to limitations of the probe of AFM system. These results reveal that the introduction of POSS effectively improve the film formability of resultant hybrid. The similar results were also observed in our previous works and other reports.[18–20]

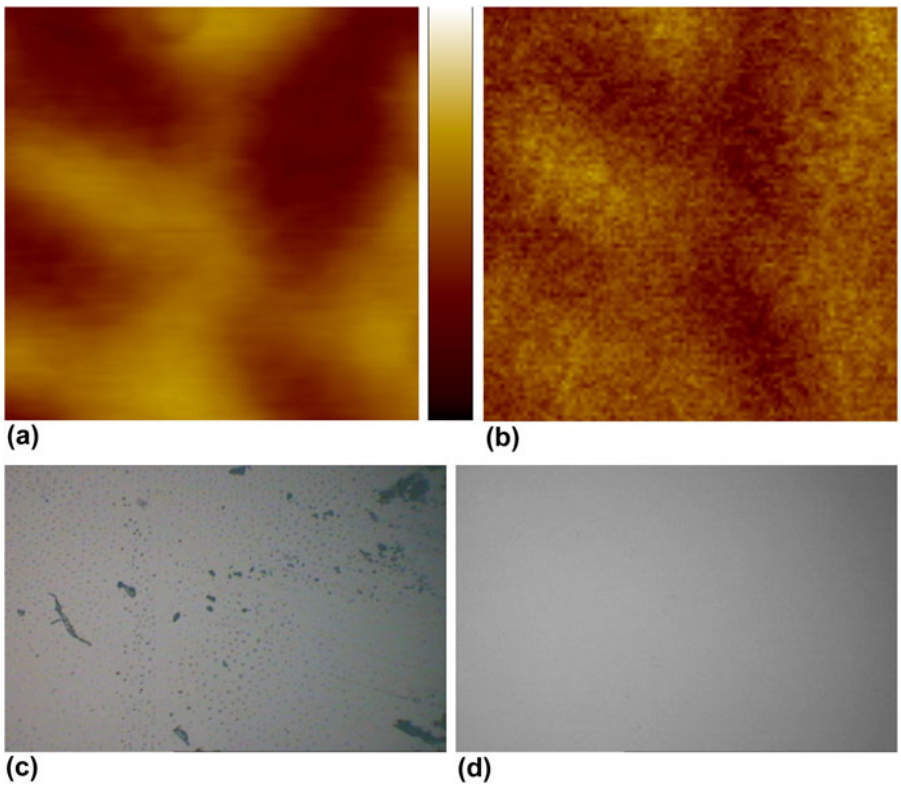


FIG. 4. 1.0 × 1.0 μm tapping mode AFM (a) height and (b) phase images for POSSAF thin film (*Z* ranges for the height and phase images are 5 nm). OM micrographs at 200× magnification: AF (c) and POSSAF (s) thin films.

https://doi.org/10.1557/jmr.2013.36 Published online by Cambridge University Press

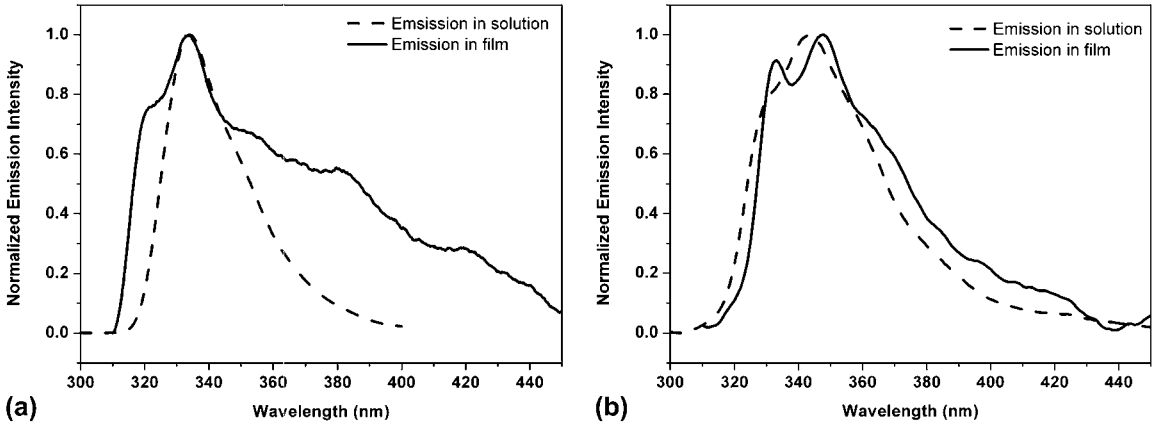


FIG. 5. Normalized emission spectra of AF (a) and POSSAF (b) in solution and in film.

E. Light-emitting and deaggregation effect of POSSAF

For investigating the influence of incorporation of POSS on optical properties of resultant organic nanoparticle, the photoluminescence spectra of the AF and POSSAF in solid film were also tested (Fig. 5). It is clearly observed that the emission spectrum of AF film obviously broadens compared with its solution spectrum, and two new emission shoulder peaks at about 316 and 380 nm appear, which are attributed to the formation of H-aggregation and J-aggregation in solid film. However, POSSAF film shows almost similar emission spectrum with its solution spectrum and only a slight red-shift is observed, indicating that the H-aggregation, and J-aggregation effects are effectively weakened. These results indict that the introduction of POSS effectively prohibits the aggregation of organic units. Simultaneously, POSSAF film exhibits more refined emitting spectral structure due to the hindrance of molecular rotation and vibration in solid state. Most importantly, although both AF and POSSAF exhibit high fluorescence quantum yield in solution (83% and 84%, respectively), POSSAF film still keeps 80% emission fluorescence quantum yield while the fluorescence quantum yield of AF film is only 14%, further confirming that the introduction of POSS into organic optical materials shows a significant disaggregating effect.

F. The thermal stability of photoluminescence of POSSAF film

The thermal stability of organic optical materials is a very important parameter for their applications. Therefore, we tested the emission spectra of AF and POSSAF thin films before and after annealing at 100 °C in air for 1 h. As seen in Fig. 6(a), the luminescence of AF film after annealing is completely quenched owing to the degradation of film and a new long-wave length emission at 470 nm appeared due to the formation of fluorenone structure.[36] However, in Fig. 6(b), the emission spectrum of POSSAF film is almost not affected. On the strength of its own validity, it is attributed to the high thermal stability of POSSAF molecules, which is further proved by the temperature-dependent IR spectra [Figs. 5(c) and 5(d)]. AF is extremely sensitive to heat. At 100 °C, all the characteristic absorptions at 3275 cm^{-1} (≡C–H), 2099 cm^{-1} (C≡C), 3036 cm^{-1} (Ar–H) and 2957, 2929, 2858 cm^{-1} (–CH) begin to extinguish and almost disappear at 200 °C owing to the decomposition of AF molecules. However, POSSAF is much more thermostable. The characteristic absorptions (–CH, triazole ring, Si–O–Si) exhibit no significant change until 300 °C. On the other hand, the amorphous stability of POSSAF film is also an important reason, i.e., there is no change in film structure during heating. This was confirmed by DSC measurement [Figs. 5(e) and 5(f)]. The DSC curve of AF exhibits a large melting peak at 70 °C, indicating that AF film is thermally unstable, which is a major drawback to film structure. However, after introduction of POSS, this thermally unstable AF has been transformed to a thermostable hybrid material and there is no melting or crystallization peak that has been observed up to 250 °C, which effectively safeguards the film stability.

The thermal properties of POSSAF were further tested by TGA (Fig. 7). Generally, the thermal decomposition behavior of POSS macromeres exhibits two-step decomposition: the decomposition of organic component and inorganic POSS cage. However, the TGA curve of POSSAF only shows one-step decomposition. Meanwhile, the $T_{d5\%}$ value of POSSAF is at approximately 264 °C, an approximate 110 °C increase from 157 °C of AF. Moreover, the char yield of the thermally cured POSSAF was 72.9%, which are much higher than that of AF (8.1%) and POSSN3 (37.9%). The thermal stability enhancement and one-step decomposition behavior are mainly attributed to the even

https://doi.org/10.1557/jmr.2013.36 Published online by Cambridge University Press

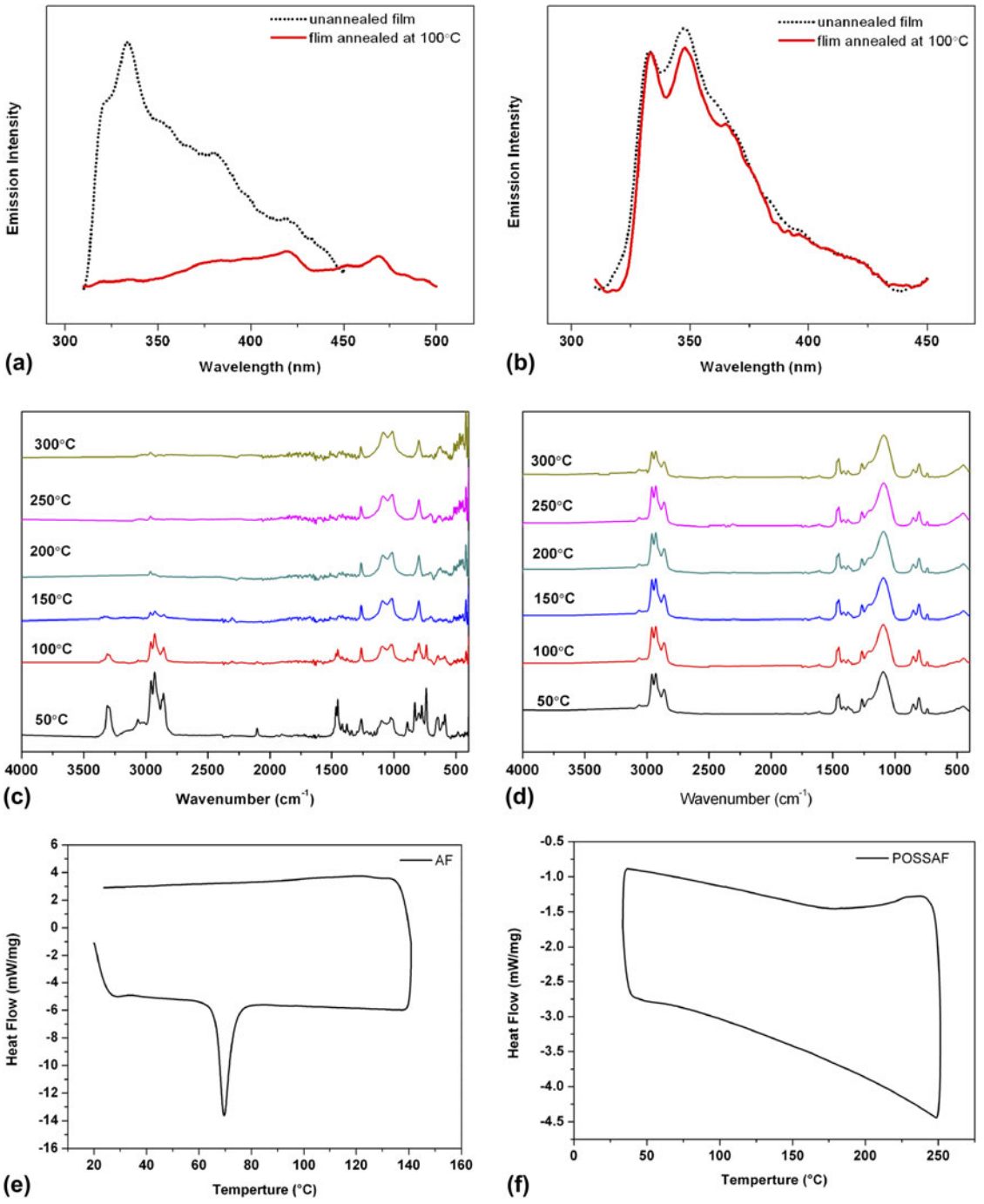


FIG. 6. Emission spectra of AF (a) and POSSAF (b) as pristine thin films and as films annealed at 100 °C in air for 1 h; temperature-dependent IR curves of AF (c) and POSSAF (d) form 50 to 300 °C, held for 30 min at each temperature; and DSC curves of AF (e) and POSSAF (f) at a heating rate of 10 °C/min and cooling rate 10 °C/min under nitrogen atmosphere, held for 10 min at the highest temperature before cooling.

dispersion of POSS at molecular level, and high thermal stability of inorganic POSS cage to hinder the heat transfer. The jacket effect of the fluorene pendants may also provide another contribution to thermal properties enhancement of resultant hybrid, in which the POSS core may have been surrounded by a rigid jacket formed through the strong intra- and intermolecular electronic interactions of the organic arms, shielding the molecules from the thermal attack.[37] Simultaneously, the triazole ring also enhances the thermal stability of the hybrid nanocomposite.[38] Furthermore, as the organic component is oxidized away from the surface, the remaining residue becomes enriched in silica and provides a barrier to further oxidation.[39]

https://doi.org/10.1557/jmr.2013.36 Published online by Cambridge University Press

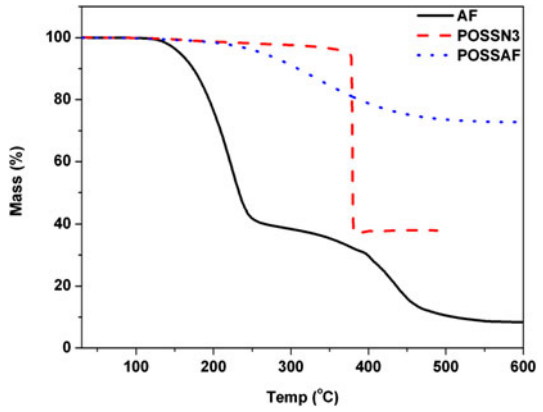


FIG. 7. Decompositon of FL, POSSN3 and POSSFL (TGA in N_2, 10 °C/min).

IV. CONCLUSIONS

In conclusion, a novel well-defined 3D POSS-based organic-inorganic hybrid material POSSAF was controllably prepared via click chemistry method. The results indicate that the introduction of POSS core can effectively prevent molecular aggregation, improve thermal stability, film formability and photophysical properties of resultant hybrid, and shows highly efficient and stable luminescence both in solvent and solid state. Meanwhile, this preparation method will ensure the emission purity of organic units and achieve a pure UV emission. This work provides a novel strategy for design of solid-state organic luminescent materials with high thermal and photophysical stability.

ACKNOWLEDGMENTS

The authors acknowledge financial support from National Natural Science Fund of China (Grant Nos. 20971021, 51003013, 51073031, 21171034, and 21271040), Doctoral Dissertation Innovation Project (Grant No. BC200901).

REFERENCES

1. K.Y. Pu and B. Liu: Conjugated polyelectrolytes as light-up macromolecular probes for heparin sensing. *Adv. Funct. Mater.* **19**, 277 (2009).
2. J. Lott, C. Ryan, B. Valle, J.R. JohnsonIII, D.A. Schiraldi, J. Shan, K.D. Singer, and C. Weder: Two-photon 3D optical data storage via aggregate switching of excimer-forming dyes. *Adv. Mater.* **23**, 2425 (2011).
3. L.T. Dou, J.B. You, J. Yang, C.C. Chen, Y.J. He, S. Murase, T. Moriarty, K. Emery, G. Li, and Y. Yang: Tandem polymer solar cells featuring a spectrally matched low-bandgap polymer. *Nat. Photonics* **6**, 180 (2012).
4. W.J. Feast and A.F.M. Kilbinger: Solution processable alternating oligothiophene-PEO-block-co-polymers: Synthesis and evidence for solvent dependent aggregation. *J. Mater. Chem.* **10**, 1777 (2000).
5. X.B. Sun, X.J. Xu, W.F. Qiu, G. Yu, H.J. Zhang, X.K. Gao, S.Y. Chen, Y.L. Song, and Y.Q. Liu: A non-planar pentaphenylbenzene functionalized benzo [2,1,3] thiadiazole derivative as a novel red molecular emitter for non-doped organic light-emitting diodes. *J. Mater. Chem.* **18**, 2709 (2008).
6. A. Lukyanov, A. Malafeev, V. Ivanov, H.L. Chen, K. Kremer, and D. Andrienko: Solvated poly-(phenylene vinylene) derivatives: Conformational structure and aggregation behavior. *J. Mater. Chem.* **20**, 10475 (2010).
7. H.T. Wang, F.Q. Bai, H.M. Liu, B.L. Bai, X. Ran, S.N. Qu, J.H. Shi, D.J. Xie, H.Y. Li, M. Li, and H.X. Zhang: Experimental and theoretical study on molecular aggregation and its effect on the photo-physical properties of the mesogenic bi-1,3,4-thiadiazole derivative. *Phys. Chem. Chem. Phys.* **13**, 9697 (2011).
8. C. Romero-Nieto, S. Merino, J. Rodriguez-Lopez, and T. Baumgartner: Dendrimeric oligo(phenylenevinylene)-extended dithieno[3,2-*b*:2′, 3′-*d*]phospholes: Synthesis, self-organization, and optical properties. *Chem. Eur. J.* **15**, 4135 (2009).
9. J. You, G.Y. Li, R.J. Wang, Q.P. Nie, Z.G. Wang, and J.Y. Li: Pyrene-cored dendrimer with carbazole derivatives as dendrons: Synthesis, properties and application in white light-emitting diode. *Phys. Chem. Chem. Phys.* **13**, 17825 (2011).
10. P.K. Lekha and E. Prasad: Tunable emission of static excimer in a pyrene-modified polyamidoamine dendrimer aggregate through positive solvatochromism. *Chem. Eur. J.* **17**, 8609 (2011).
11. J.F. Ma, L.P. Zhang, J. Yang, Y.Y. Liu, and G.H. Wei: 1D, 2D, and 3D metal-organic frameworks based on bis(imidazole) ligands and polycarboxylates: Syntheses, structures, and photoluminescent properties. *Cryst. Growth Des.* **9**, 4660 (2009).
12. B. Trastoy, M.E. Perez-Ojeda, R. Sastre, and J.L. Chiara: Octakis (3-azidopropyl)octasilsesquioxane: A versatile nanobuilding block for the efficient preparation of highly functionalized cube-octameric polyhedral oligosilsesquioxane frameworks through click assembly. *Chem. Eur. J.* **16**, 3833 (2010).
13. H.P. You, K. Liu, Y.H. Zheng, G. Jia, Y.H. Song, Y.J. Huang, M. Yang, J.J. Jia, N. Guo, and H.J. Zhang: Facile and rapid fabrication of metal-organic framework nanobelts and color-tunable photoluminescence properties. *J. Mater. Chem.* **20**, 3272 (2010).
14. M.A. Mintzer and M.W. Grinstaff: Biomedical applications of dendrimers: A tutorial. *Chem. Soc. Rev.* **40**, 173 (2011).
15. X.H. Yang, J.D. Froehlich, H.S. Chae, S. Li, A. Mochizuki, and G.E. Jabbour: Novel orange-red light-emitting polymers with cyclometaled iridium complex grafted in alkyl chain. *Adv. Funct. Mater.* **19**, 2623 (2009).
16. K. Tanaka and Y. Chujo: Advanced functional materials based on polyhedral oligomeric silsesquioxane (POSS). *J. Mater. Chem.* **22**, 1733 (2012).
17. F.K. Wang, X.H. Lu, and C.B. He: Some recent developments of polyhedral oligomeric silsesquioxane (POSS)- based polymeric materials. *J. Mater. Chem.* **21**, 2775 (2011).
18. Z.Q. Yan, H.Y. Xu, S.Y. Guang, X. Zhao, W. Fan, and X.Y. Liu: A convenient organic–inorganic hybrid approach toward highly stable squaraine dyes with reduced H-aggregation. *Adv. Funct. Mater.* **22**, 345 (2012).
19. X. Wang, S.Y. Guang, H.Y. Xu, X.Y. Su, J.Y. Yang, Y.L. Song, N.B. Lin, and X.Y. Liu: Thermally stable oxadiazole-containing polyacetylenes: Relationship between molecular structure and nonlinear optical properties. *J. Mater. Chem.* **18**, 4204 (2008).
20. Y.L. Chu, C.C. Cheng, Y.P. Chen, Y.C. Yen, and F.C. Chang: A new supramolecular POSS electroluminescent material. *J. Mater. Chem.* **22**, 9285 (2012).
21. Y.C. Wu and S.W. Kuo: Self-assembly supramolecular structure through complementary multiple hydrogen bonding of heteronucleobase-multifunctionalized polyhedral oligomeric silsesquioxane (POSS) complexes. *J. Mater. Chem.* **22**, 2982 (2012).
22. B.H. Yang, H.Y. Xu, Z.Z. Yang, and C. Zhang: Controllable preparation of ultra-low-dielectric nanoporous silica via inorganic-organic hybrid templates. *J. Mater. Chem.* **20**, 2469 (2010).

https://doi.org/10.1557/jmr.2013.36 Published online by Cambridge University Press

23. X.Y. Su, S.Y. Guang, C.W. Li, H.Y. Xu, X.Y. Liu, X. Wang, and Y.L. Song: Molecular hybrid optical limiting materials from polyhedral oligomer silsesquioxane: Preparation and relationship between molecular structure and properties. *Macromolecules* **43**, 2840 (2010).
24. C. Zhang, S.Y. Guang, X.B. Zhu, H.Y. Xu, X.Y. Liu, and M.H. Jiang: Mechanism of dielectric constant variation of POSS-based organic-inorganic molecular hybrids. *J. Phys. Chem. C* **114**, 22455 (2010).
25. B.H. Yang, H.Y. Xu, Z.Z. Yang, and X.Y. Liu: Design and architecture of low-dielectric-constant organic-inorganic hybrids from octahydridosilsesquioxanes. *J. Mater. Chem.* **19**, 9038 (2009).
26. X.Y. Su, S.Y. Guang, H.Y. Xu, X.Y. Liu, S. Li, X. Wang, Y. Deng, and P. Wang: Controllable preparation and optical limiting properties of POSS-based functional hybrid nanocomposites with different molecular architectures. *Macromolecules* **42**, 8969 (2009).
27. Y.K. Zhu, S.Y. Guang, and H.Y. Xu: A versatile nanobuilding precursor for the effective architecture of well-defined organic/inorganic hybrid via click chemistry. *Chin. Chem. Lett.* **73**, 1095 (2012).
28. R. Gujadhur, D. Venkataraman, and J.T. Kintigh: Formation of aryl–nitrogen bonds using a soluble copper(I) catalyst. *Tetrahedron Lett.* **42**, 4791 (2001).
29. J.C. Scaiano: *Handbook of Organic Photochemistry* (CRC Press, Boca Raton, FL, 1989).
30. L.L. Pleux, Y. Pellegrin, E. Blart, F. Odobel, and A. Harriman: Long-lived, charge-shift states in heterometallic, porphyrin-based dendrimers formed via click chemistry. *J. Phys. Chem. A* **115**, 5069 (2011).
31. L. Luo and C.D. Frisbie: Length-dependent conductance of conjugated molecular wires synthesized by stepwise "click" chemistry. *J. Am. Chem. Soc.* **132**, 8854 (2010).
32. A. Wild, C. Friebe, A. Winter, M.D. Hager, U.W. Grummt, and U.S. Schubert: π-conjugated 2,2′:6′,2′′-bis(terpyridines): Systematical tuning of the optical properties by variation of the linkage between the terpyridines and the π-conjugated system. *Eur. J. Org. Chem.* **2010**, 1859 (2010).
33. C. Saravanan, S. Senthil, and P. Kannan: Click chemistry-assisted triazole-substituted azobenzene and fulgimide units in the pendant-based copoly(decylozymethacrylate)s for dual-mode optical switches. *J. Polym. Sci., Part A: Polym. Chem.* **46**, 7843 (2008).
34. T.T. Lin, C. He, and Y. Xiao: Theoretical studies of monosubstituted and higher phenyl-substituted octahydrosilsesquioxanes. *J. Phys. Chem. B* **107**, 13788 (2003).
35. M.J. Frisch, G.W. Trucks, H.B. Schlegel, G.E. Scuseria, M.A. Robb, J.R. Cheeseman, J.A.J. Montgomery, T. Vreven, K.N. Kudin, J.C. Burant, J.M. Millam, S.S. Iyengar, J. Tomasi, V. Barone, B. Mennucci, M. Cossi, G. Scalmani, N. Rega, G.A. Petersson, H. Nakatsuji, M. Hada, M. Ehara, K. Toyota, R. Fukuda, J. Hasegawa, M. Ishida, T. Nakajima, Y. Honda, O. Kitao, H. Nakai, M. Klene, X. Li, J.E. Knox, H.P. Hratchian, J.B. Cross, V. Bakken, C. Adamo, J. Jaramillo, R. Gomperts, R.E. Stratmann, O. Yazyev, A.J. Austin, R. Cammi, C. Pomelli, J.W. Ochterski, P.Y. Ayala, K. Morokuma, G.A. Voth, P. Salvador, J.J. Dannenberg, V.G. Zakrzewski, S. Dapprich, A.D. Daniels, M.C. Strain, O. Farkas, D.K. Malick, A.D. Rabuck, K. Raghavachari, J.B. Foresman, J.V. Ortiz, Q. Cui, A.G. Baboul, S. Clifford, J. Cioslowski, B.B. Stefanov, G. Liu, A. Liashenko, P. Piskorz, I. Komaromi, R.L. Martin, D.J. Fox, T. Keith, M.A. Al-Laham, C.Y. Peng, A. Nanayakkara, M. Challacombe, P.M.W. Gill, B. Johnson, W. Chen, M.W. Wong, C. Gonzalez, J.A. Pople, *Gaussian 03, Revision A.1* (Gaussian, Inc., Pittsburgh, PA, 2004).
36. R. Grisorio, G.P. Suranna, P. Mastrorilli, and C.F. Nobile: Insight into the role of oxidation in the thermally induced green band in fluorene-based systems. *Adv. Funct. Mater.* **17**, 538 (2007).
37. S.C. Yin, H.Y. Xu, X.Y. Su, G. Li, Y.L. Song, J. Lam, and B.Z. Tang: Optical-limiting and nonlinear optical polyacetylenes: Synthesis of azobenzene-containing poly(1-alkyne)s with different spacer and tail lengths. *J. Polym. Sci., Part A: Polym. Chem.* **44**, 2346 (2006).
38. L. Xue, L.Q. Wan, Y.H. Hu, X.N. Shen, F.H. Huang, and L. Du: Thermal stability of a novel polytriazole resin. *Thermochim. Acta* **448**, 147 (2006).
39. S. Sulaiman, A. Bhaskar, J. Zhang, R. Guda, T. Goodson, and R.M. Laine: Molecules with perfect cubic symmetry as nanobuilding blocks for 3-D assemblies. Elaboration of octavinylsilsesquioxane. Unusual luminescence shifts may indicate extended conjugation involving the silsesquioxane core. *Chem. Mater.* **20**, 5563 (2008).

https://doi.org/10.1557/jmr.2013.36 Published online by Cambridge University Press